



Mitochondrial Safeguard: a stress response that offsets extreme fusion and protects respiratory function via flickering-induced Oma1 activation

Daisuke Murata¹ , Tatsuya Yamada¹, Takeshi Tokuyama¹, Kenta Arai¹, Pedro M Quirós², Carlos López-Otín², Miho Iijima^{1,*} & Hiromi Sesaki^{1,**} 

Abstract

The connectivity of mitochondria is regulated by a balance between fusion and division. Many human diseases are associated with excessive mitochondrial connectivity due to impaired Drp1, a dynamin-related GTPase that mediates division. Here, we report a mitochondrial stress response, named mitochondrial safeguard, that adjusts the balance of fusion and division in response to increased mitochondrial connectivity. In cells lacking Drp1, mitochondria undergo hyperfusion. However, hyperfusion does not completely connect mitochondria because Opa1 and mitofusin 1, two other dynamin-related GTPases that mediate fusion, become proteolytically inactivated. Pharmacological and genetic experiments show that the activity of Oma1, a metalloprotease that cleaves Opa1, is regulated by short pulses of the membrane depolarization without affecting the overall membrane potential in Drp1-knockout cells. Re-activation of Opa1 and Mitofusin 1 in Drp1-knockout cells further connects mitochondria beyond hyperfusion, termed extreme fusion, leading to bioenergetic deficits. These findings reveal an unforeseen safeguard mechanism that prevents extreme fusion of mitochondria, thereby maintaining mitochondrial function when the balance is shifted to excessive connectivity.

Keywords Drp1; mitochondrial fusion; mitofusin; Oma1; Opa1

Subject Categories Membranes & Trafficking; Organelles

DOI 10.15252/embj.2020105074 | Received 23 March 2020 | Revised 15 October 2020 | Accepted 22 October 2020 | Published online 17 November 2020

The EMBO Journal (2020) 39: e105074

See also: **LC Tábara & J Prudent** (December 2020)

Introduction

The mitochondrion is an essential organelle for a variety of cellular processes, including energy production, metabolism, and signal transduction. These mitochondrial functions depend on

mitochondrial morphology (Kameoka *et al.*, 2018). In many cell types, mitochondria form short tubular structures with branches. The morphology of mitochondria is governed by a dynamic balance between mitochondrial fusion and division (Youle & van der Blik, 2012; Friedman & Nunnari, 2014; Kashatus, 2018; Widlansky & Hill, 2018). Fusion merges two separate mitochondria, and division separates single mitochondrion into two. Unbalanced excess fusion or division leads to enlargement or fragmentation of mitochondria, respectively.

In humans, mutations in a conserved mitochondrial division GTPase, Drp1 (McNiven *et al.*, 2000; Tamura *et al.*, 2011; van der Blik *et al.*, 2013; Pernas & Scorrano, 2016; Kraus & Ryan, 2017; Prudent & McBride, 2017; Kameoka *et al.*, 2018; Ramachandran, 2018), lead to mitochondrial division defects, mitochondrial enlargement, and neurodevelopmental and neurodegenerative disorders (Itoh *et al.*, 2013; Liesa & Shirihai, 2013; Roy *et al.*, 2015; Serasinghe & Chipuk, 2017). In addition to Drp1, defects in its mitochondrial receptor protein, Mff, are associated with neuropathy (Itoh *et al.*, 2013; Liesa & Shirihai, 2013; Roy *et al.*, 2015; Serasinghe & Chipuk, 2017). Like the nervous system, giant mitochondria, termed megamitochondria, are formed in hepatocytes of the liver in patients with alcoholic and nonalcoholic fatty liver diseases (Kleiner & Makhlof, 2016). Recapitulating these human liver diseases, a mouse model for nonalcoholic steatohepatitis produces megamitochondria in hepatocytes (Yamada *et al.*, 2018). Suppressing megamitochondria formation by blocking mitochondrial fusion mitigates liver damage in this mouse model, suggesting a pathogenic role of megamitochondria (Yamada *et al.*, 2018).

Enlargement of mitochondria due to decreased division compromises their transport in cells and, therefore, causes uneven distribution of mitochondria (Roy *et al.*, 2015; Kameoka *et al.*, 2018). This is particularly evident in neurons, which form long cytoplasmic extensions, such as dendrites and axons, and many small projections along dendrites, such as spines (Li *et al.*, 2004; Kageyama *et al.*, 2012; Itoh *et al.*, 2013; Shields *et al.*, 2015; Divakaruni *et al.*, 2018). In addition to defects in transport and distribution, enlarged mitochondria become defective in autophagic degradation. Their oversize

¹ Department of Cell Biology, Johns Hopkins University School of Medicine, Baltimore, MD, USA

² Departamento de Bioquímica y Biología Molecular, Facultad de Medicina, Instituto Universitario de Oncología, Universidad de Oviedo, Oviedo, Spain

*Corresponding author. Tel: +1 410 502 6836; E-mail: miiijima@jhmi.edu

**Corresponding author. Tel: +1 410 502 6842; E-mail: hsesaki@jhmi.edu

makes mitochondria resistant to autophagosomal engulfment during mitophagy, leading to the accumulation of ubiquitinated mitochondria in the brain, liver, and heart (Twig *et al*, 2008; Kageyama *et al*, 2012; Kageyama *et al*, 2014; Yamada *et al*, 2018).

Interestingly, mitochondrial division appears to be coupled to mitochondrial fusion. In multiple types of cells, including neurons, hepatocytes, and fibroblasts, the enlargement of mitochondria as the consequence of the lack of mitochondrial division causes decreases in the level of mitofusin 1 and 2 (Mfn1 and 2), two homologous mitochondrial fusion GTPases in the outer membrane (Ishihara *et al*, 2009; Wakabayashi *et al*, 2009; Kageyama *et al*, 2014; Saita *et al*, 2016; Yamada *et al*, 2018; Yamada *et al*, 2019). The degradation of Mfn1 and 2 in the absence of Drp1 is controlled by two proteins that are associated with Parkinson's disease, parkin (a ubiquitin E3 ligase) and PINK1 (a mitochondrial protein kinase that activates parkin and ubiquitin by phosphorylating these proteins) in the liver (Yamada *et al*, 2018; Yamada *et al*, 2019). Also, Opa1, another mitochondrial fusion GTPase in the inner membrane, is proteolytically cleaved in the absence of Drp1 (Ishihara *et al*, 2009; Mopert *et al*, 2009; Wakabayashi *et al*, 2009; Saita *et al*, 2016; Yamada *et al*, 2018; Yamada *et al*, 2019). The cleavage of Opa1 is mediated by the metalloprotease Oma1 (Ehnes *et al*, 2009; Head *et al*, 2009; Quiros *et al*, 2012; Baker *et al*, 2014; Zhang *et al*, 2014; Rainbolt *et al*, 2016; Acin-Perez *et al*, 2018). Currently, it is unknown how these proteolytic mechanisms are activated, whether these mechanisms suppress fusion, and what the functional importance of the mechanisms might be.

Here, we report that, in the absence of mitochondrial division in Drp1-knockout (KO) cells, Oma1 is tuned to be partially activated in a restricted fashion by repeated, transient decreases of the mitochondrial membrane potential, called flickering, without losing the overall membrane potential. Furthermore, preventing Opa1 cleavage together with ectopic expression of Mfn1 induced further mitochondrial fusion in Drp1-KO cells. We termed this status of over fused mitochondria extreme fusion of mitochondria, to distinguish from hyperfusion, which has been used to refer to connected mitochondria due to decreased division. The extreme fusion of mitochondria results in a dramatic loss of the membrane potential and respiration. Thus, mitochondria use flickering as a safeguard mechanism that prevents more deleterious extreme fusion, beyond hyperfusion, when mitochondrial division is blocked.

Results

Opa1 is encoded by the single gene and produces multiple isoforms via alternative mRNA splicing and proteolytic processing (MacVicar & Langer, 2016; Kameoka *et al*, 2018). In wild-type (WT) mouse embryonic fibroblasts (MEFs), five isoforms, including two long forms (L1 and L2) and three short forms (S3, S4, and S5), were detected by Western blotting (Fig 1A and B). S3 and S5 are produced by proteolytic cleavage of L1 and L2, respectively, via the inner membrane metalloprotease Oma1 (Fig 1A) (Ehnes *et al*, 2009; Head *et al*, 2009; MacVicar & Langer, 2016; Kameoka *et al*, 2018). Since Oma1 is activated by the loss of the mitochondrial membrane potential (Ehnes *et al*, 2009; Head *et al*, 2009), a proton ionophore, trifluoromethoxy carbonyl cyanide phenylhydrazine (FCCP), which

dissipates the membrane potential, converted essentially all of L1 and L2 to S3 and S5 (Fig 1B and C). In contrast, FCCP did not affect the production of S4 (Fig 1B and C), consistent with the previous observation that S4 is produced by the proteolytic cleavage of L1 by another inner membrane AAA protease, Yme1L, independently of the membrane potential (Fig 1A) (Song *et al*, 2007; Anand *et al*, 2014). The effect of FCCP was specific to Opa1. We observed no changes for other mitochondrial fusion or division proteins (Fig 1B and C).

Amounts of L1 and L2 were decreased in Drp1-KO MEFs compared with WT MEFs, while those of S3 and S5 were increased (Fig 1B and C). In contrast, the level of S4 appeared unaffected (Fig 1B and C). We also observed decreases in the amounts of Mfn1 and Mfn2. In contrast to these mitochondrial fusion proteins, Drp1 receptor proteins, such as Mff, Fis1, Mid49, and Mid51, were unaffected in Drp1-KO MEFs (Fig 1B and C). The increased conversion of Opa1 and the decreased levels of Mfn1 and Mfn2 were rescued by the re-expression of Drp1 (Fig 1B and C).

An experimental system to analyze Opa1 processing

To investigate the mechanism by which the conversion of the long forms (L1 and L2) to the short forms (S3 and S5) is increased in Drp1-KO cells, we simplified our experimental platform by ectopically expressing HA-tagged L2 (L2-HA) from the tetracycline-inducible promoter (Fig 2A). Similar to endogenous L2, the conversion of L2-HA to S5-HA was increased in Drp1-KO MEFs (Fig 2B and C). The re-expression of Drp1 restored a normal level of conversion of L2-HA to S5-HA (Fig 2B and C).

Western blotting showed that the level of Oma1 was decreased in Drp1-KO MEFs (Fig 2B and C). As a readout for Oma1 activation, the loss of full-length Oma1 has been used since Oma1 becomes active by self-cleavage, which is followed by degradation (Fig 2D) (Ehnes *et al*, 2009; Head *et al*, 2009; Zhang *et al*, 2014; MacVicar & Langer, 2016). Indeed, FCCP, which activates Oma1, greatly decreased the level of Oma1 (Fig 2B and C). Therefore, decreased levels of Oma1 in Drp1-KO MEFs suggest its partial activation. Re-expression of Drp1 in Drp1-KO MEFs restored the normal level of Oma1 (Fig 2B and C). To test whether the conversion of L2-HA to S5-HA requires Oma1, we knocked down Oma1 using shRNAs (Fig 2E and F). The Oma1 knockdown blocked the L2-HA to S5-HA conversion in Drp1-KO MEFs (Fig 2E and F). The FCCP-induced Opa1 processing was also inhibited by Oma1 knockdown in both WT and Drp1-KO MEFs (Fig 2E and F).

Blocking flickering by antimycin A decreases Opa1 processing, while stimulating by oligomycin flickering increases Opa1 processing in Drp1-KO cells

Although Oma1 can be activated by the loss of the membrane potential, as described above, Drp1-KO MEFs showed normal overall membrane potential as measured by flow cytometry (Fig 3A). However, the membrane potential showed transient drops, termed flickering, in Drp1-KO MEFs when observed by time-lapse microscopy using a membrane potential-dependent dye, tetramethylrhodamine ethyl ester (TMRE) (Fig 3B and C; Movies EV1–EV4; Galloway *et al*, 2012; Lee & Yoon, 2014; Roy *et al*, 2016). In WT MEFs, flickering was almost undetectable (Fig 3C and K; Movie

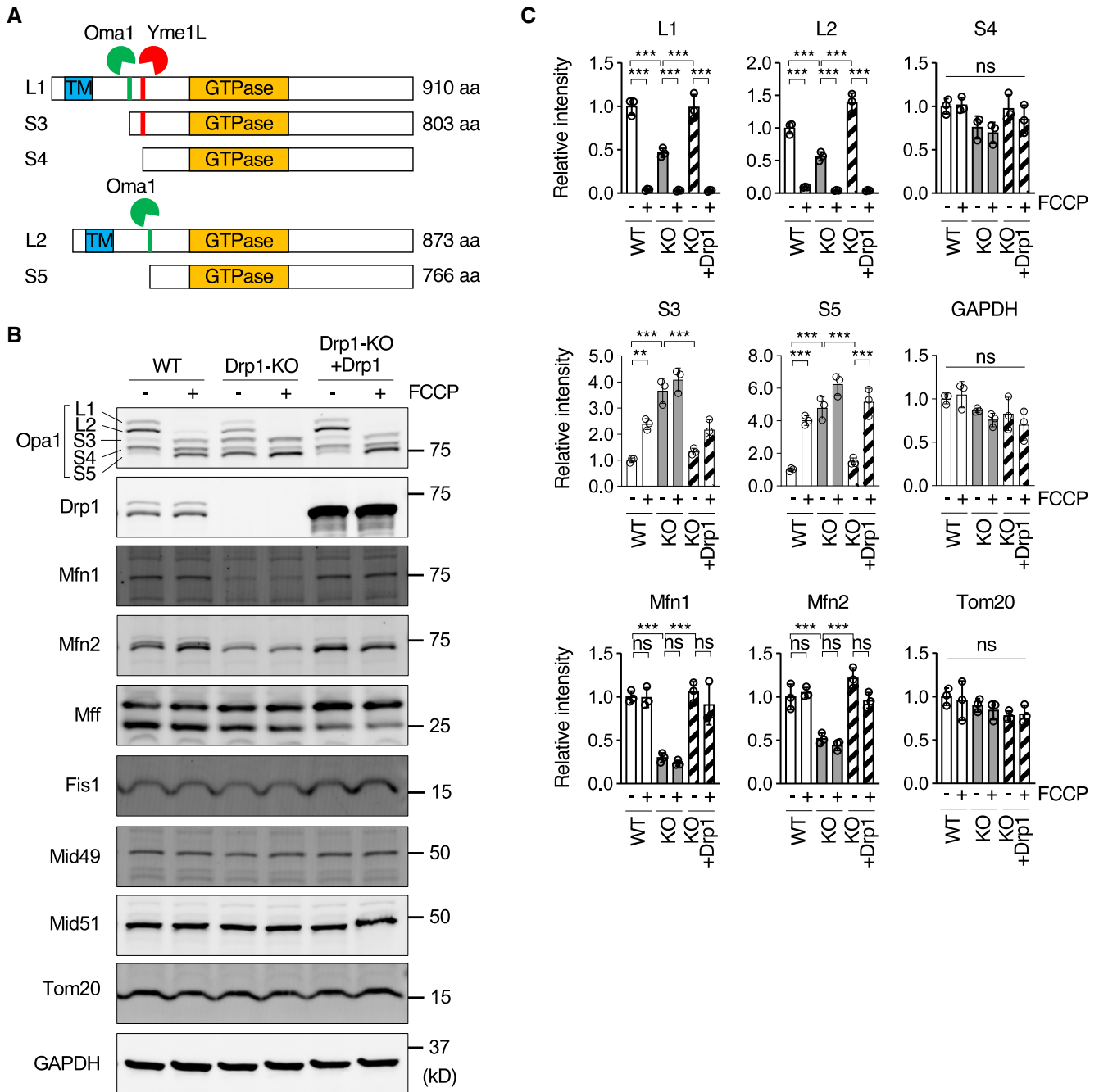


Figure 1. Increased conversion of long isoforms of Opa1 to short forms in Drp1-KO MEFs.

A Proteolytic processing of Opa1. L1 is cleaved by both Oma1 and Yme1L, while L2 is only cleaved by Oma1.

B Western blotting of WT and Drp1-KO MEFs with or without FCCP treatment (30 min) using the indicated antibodies.

C Quantification of band intensity. Values are average \pm SD ($n = 3$). Significance was calculated using ANOVA with *post hoc* Tukey: ** $P < 0.01$, *** $P < 0.001$.

EV1; Roy *et al*, 2016). Similar to knockout of Drp1, knockdown of Drp1 also induced flickering in Drp1 knockdown MEFs (Fig 3D and Appendix Fig S1), suggesting that flickering is not an adaptation to the chronic loss of Drp1. To ask whether the induction of flickering is specific to Drp1 loss, we knocked out Mff, a major Drp1 receptor. We observed increased flickering in Mff-KO MEFs (Fig 3E and

Appendix Fig S2). These data suggest flickering is induced by decreases in mitochondrial division and is not limited to Drp1 loss.

We reasoned that flickering might induce the conversion of Opa1 long forms to short forms in Drp1-KO MEFs by partially activating Oma1. To test this possibility, we inhibited or activated flickering and examined Opa1 processing. It has been

shown that antimycin A, an inhibitor of Complex III (coenzyme Q—cytochrome *c* reductase), decreases flickering in Drp1-KO MEFs (Lee & Yoon, 2014; Fig 3B and C; Movies EV2 and EV3). In contrast, oligomycin, an inhibitor of Complex V (ATP

synthase), increases the frequency of flickering in Drp1-KO MEFs (Lee & Yoon, 2014; Fig 3B and C; Movies EV2 and EV4). Before treatment with antimycin A or oligomycin, we measured the activity of Complexes III and V in WT and Drp1-KO MEFs. We

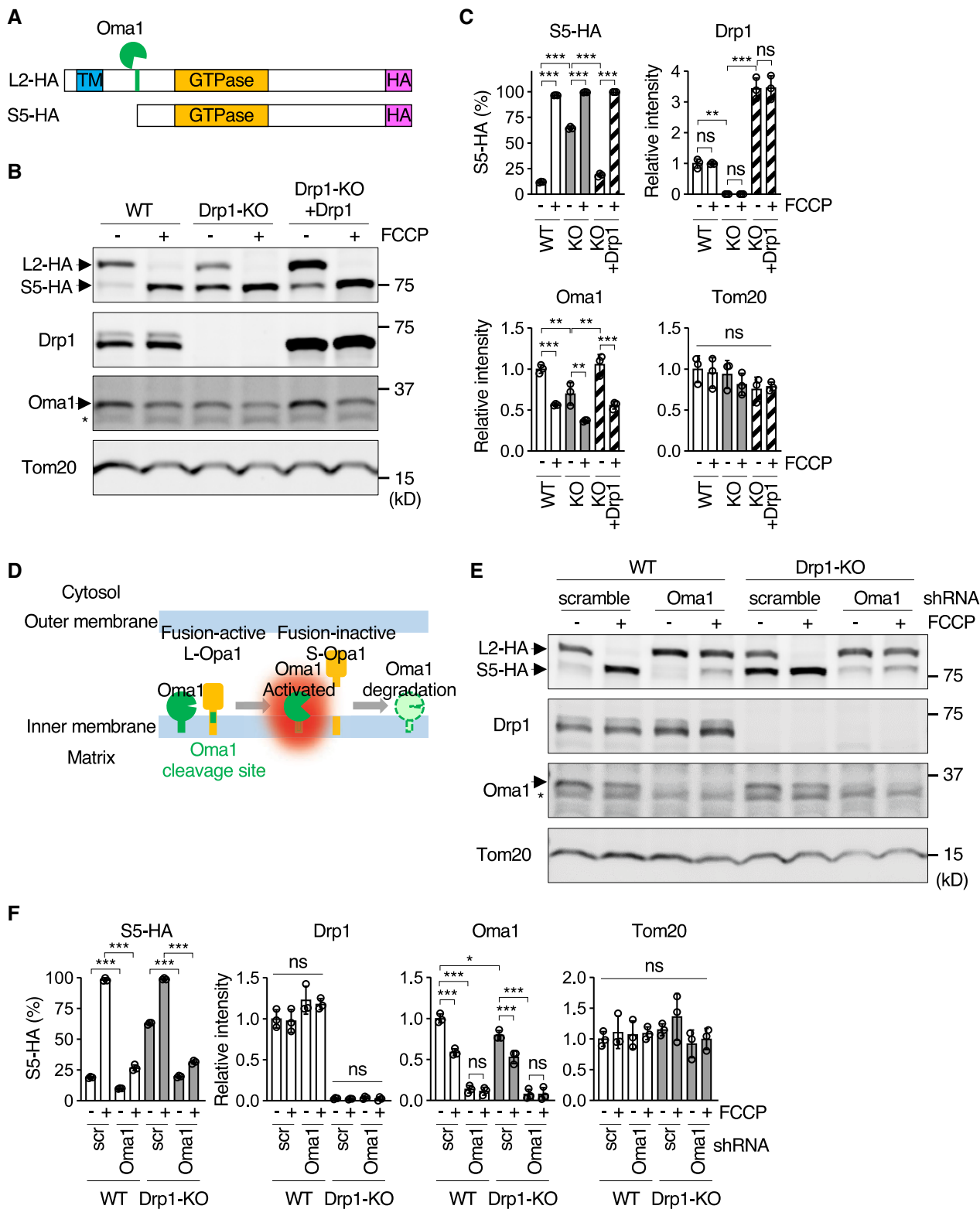


Figure 2.

Figure 2. An experimental system to examine Opa1 processing.

- A L2 was tagged with HA at the C terminus and expressed from the doxycycline-inducible promoter.
 B Western blotting of WT MEFs, Drp1-KO MEFs, and Drp1-KO MEFs carrying Drp1, all of which express L2-HA, using the indicated antibodies. The expression of L2-HA was induced for 16 h (0.1 μ g/ml doxycycline). The asterisk indicates non-specific bands of anti-Oma1 antibodies.
 C Quantification of band intensity. Values are average \pm SD ($n = 3$).
 D The activation of Oma1. Oma1 is proteolytically activated and then undergoes degradation.
 E WT and Drp1-KO MEFs, both of which express L2-HA, were transduced with lentiviruses carrying either scramble or Oma1-targeted shRNAs. Whole-cell lysates were analyzed by Western blotting using the indicated antibodies. The asterisk indicates non-specific bands of anti-Oma1 antibodies.
 F Quantification of band intensity. Values are average \pm SD ($n = 3$).

Data information: Significance was calculated using ANOVA with *post hoc* Tukey in (C and F): * $P < 0.05$, ** $P < 0.01$, *** $P < 0.001$.

found similar activities for both complexes in these MEFs (Appendix Fig S3).

First, the treatment of Drp1-KO MEFs with 10 nM antimycin A did not change the overall membrane potential (Fig 3F). Western blotting showed that antimycin A decreases the conversion of L2-HA to S5-HA (Fig 3G and H). When the mitochondrial membrane potential was dissipated with FCCP, most L2-HA was processed to S5-HA in Drp1-KO MEFs in the presence of antimycin A (Fig 3G and H). Second, the treatment of Drp1-KO MEFs with 10 ng/ml oligomycin did not affect the overall membrane potential (Fig 3F). Western blotting showed that oligomycin enhanced the processing of L2-HA to S5-HA in Drp1-KO MEFs (Fig 3I and J). Consistent with increased Opa1 processing, amounts of Oma1 were decreased in Drp1-KO MEFs in the presence of oligomycin (Fig 3I and J). These data suggest that Opa1 processing is inhibited when flickering is blocked while the processing is activated when flickering is enhanced. Furthermore, when we measured oxygen consumption rates (OCRs), both antimycin A and oligomycin decreased basal OCRs in Drp1-KO MEFs (Appendix Fig S4). Therefore, changes in OCRs do not correlate with the flickering frequency or Opa1 processing.

When we treated WT MEFs with oligomycin, we found increases in both flickering and Opa1 processing (Fig 3K–M). It appears that oligomycin-induced flickering is independent of mitochondrial morphology and can induce Opa1 processing.

Repressing flickering by Opa1 knockout decrease Opa1 processing

It has been shown that Opa1 is required for flickering in Drp1-KO MEFs (Lee & Yoon, 2014). Indeed, Drp1Opa1 double knockout MEFs, which were created by expressing Cre recombinase in Drp1^{flox/flox}Opa1^{flox/flox} MEFs, displayed no flickering similar to parent Drp1^{flox/flox}Opa1^{flox/flox} MEFs (Fig 4A–C). Consistent with the role of flickering in Oma1 activation, similar levels of Oma1 were found in Drp1Opa1-KO and Drp1^{flox/flox}Opa1^{flox/flox} MEFs (Fig 4A and B).

Confocal immunofluorescence microscopy using antibodies to a mitochondrial protein, pyruvate dehydrogenase (PDH), showed that Drp1Opa1-KO MEFs displayed relatively normal mitochondrial morphology similar to control Drp1^{flox/flox}Opa1^{flox/flox} MEFs (Fig 4D and E). These data support the notion that mitochondrial morphology is antagonistically regulated by division and fusion, but these two activities are not essential for mitochondrial morphogenesis, consistent with our previous reports in which mitochondrial morphology is restored in Drp1Opa1 double knockout hepatocytes in the mouse liver (Yamada *et al*, 2018; Yamada *et al*, 2019) and in

yeast mutants which lack both mitochondrial division and fusion proteins (Sesaki & Jensen, 1999, 2001; Sesaki *et al*, 2003).

We then transduced Drp1Opa1-KO MEFs with lentiviruses carrying WT L2-HA or two mutants that have a point mutation in the essential GTPase domain, L2(K301A)-HA or L2(K468D)-HA (Griparic *et al*, 2004; Dadgar *et al*, 2006), under the doxycycline-inducible promoter (Fig 4F). At 16 h after the induction of Opa1 expression, we analyzed mitochondrial morphology using immunofluorescence microscopy with anti-PDH antibodies. The mitochondrial localization of all of the Opa1-HA proteins was confirmed (Appendix Fig S5). The re-expression of WT L2-HA changed mitochondria from normal morphology to more elongated morphology in Drp1Opa1-KO MEFs, similar to single Drp1-KO MEFs (Fig 4D and E). In contrast, neither L2(K301A)-HA nor L2(K468D)-HA changed mitochondrial morphology, suggesting that these mutations block mitochondrial fusion (Fig 4D and E).

Expression of WT L2-HA increased flickering in Drp1Opa1-KO MEFs, like Drp1-KO MEFs (Fig 4C). In contrast, L2(K301A)-HA or L2(K468D)-HA failed to do so. We then examined the processing of these Opa1 mutants. In Drp1Opa1-KO MEFs, WT L2-HA showed increased conversion to S5-HA (Fig 4G and H). In contrast, the processing of L2(K301A)-HA or L2(K468D)-HA was not increased. When we treated these cells with FCCP, all of these Opa1 proteins underwent proteolytic processing (Fig 4G and H). As a control, WT L2-HA, L2(K301A)-HA, and L2(K468D)-HA showed similar, low levels of conversion to S5 in Drp1^{flox/flox}Opa1^{flox/flox} MEFs (Fig 4G and H). Therefore, the mutations that block flickering inhibit Opa1 cleavage.

In addition to mitochondrial fusion, Opa1 functions in the structure of inner membrane cristae (Pernas & Scorrano, 2016). To test whether alterations in cristae morphology block flickering, we knocked down Mic60, a major component of the mitochondrial contact site and cristae organizing system (Stephan *et al*, 2020). We found that Mic60 knockdown increases flickering, instead of decreasing it, in Drp1-KO MEFs (Appendix Fig S6). These data suggest that the role of Opa1 in mitochondrial fusion, rather than in cristae morphology, is important for flickering.

Artificial flickering induces Opa1 cleavage

The pharmacological and genetic experiments described above suggest that flickering promotes the proteolytic cleavage of Opa1 in the absence of Drp1. To test whether flickering is sufficient to drive Opa1 cleavage, we artificially induced flickering in WT MEFs by repeating the addition and removal of FCCP in the culture medium (Fig 5A). By testing different concentrations of FCCP and durations of FCCP treatment, we optimized the experimental condition to drop

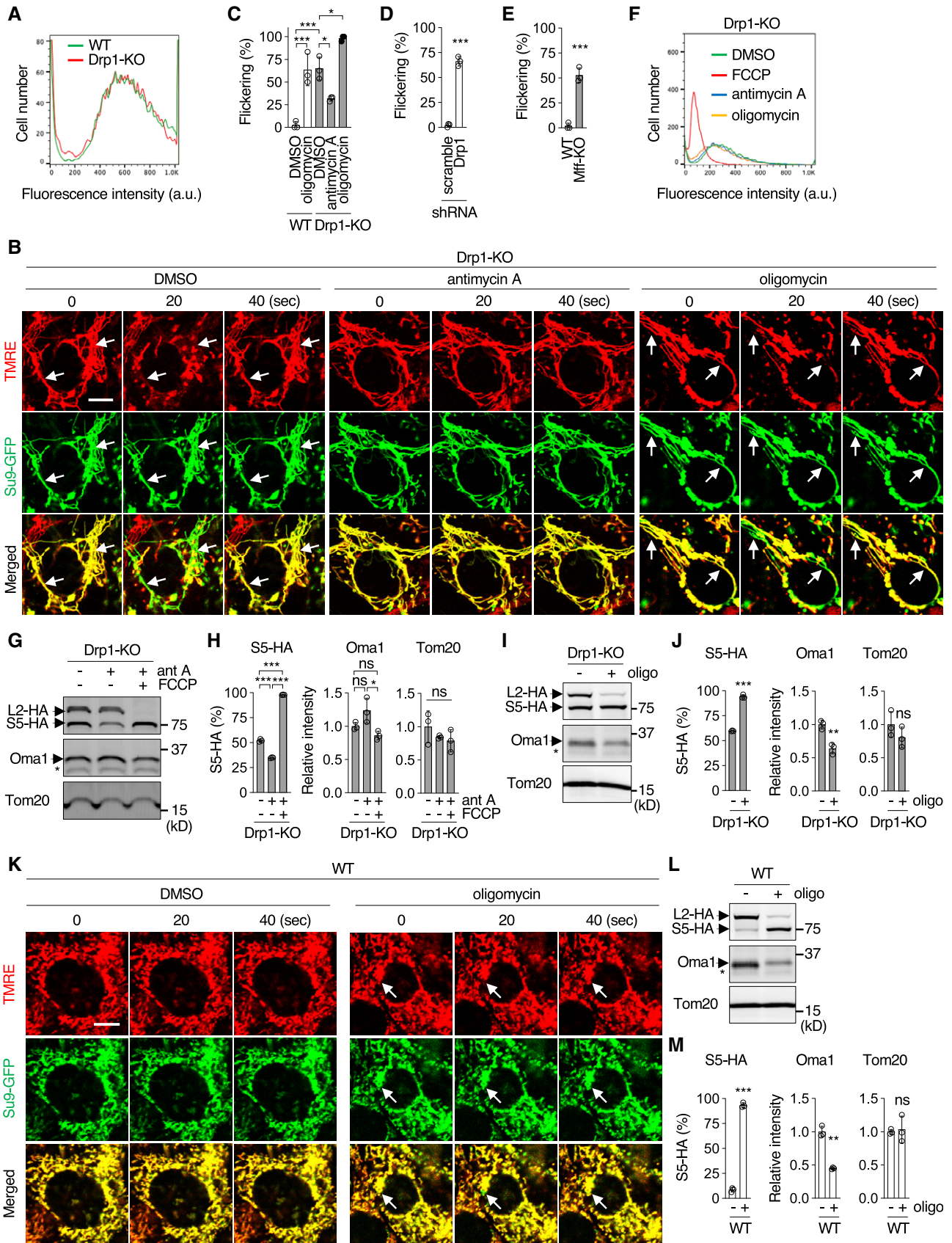


Figure 3.

Figure 3. Effects of antimycin A (10 nM) and oligomycin (10 ng/ml) on flickering and Opa1 cleavage in Drp1-KO MEFs.

- A The mitochondrial membrane potential was measured in WT and Drp1-KO MEFs using a membrane potential-dependent dye (MitoLite NIR) and flow cytometry.
- B Drp1-KO MEFs carrying Su9-GFP were treated with DMSO (control) or 10 nM antimycin A or 10 ng/ml oligomycin for 1 h and viewed by laser scanning confocal microscopy for 30 min with 10-s intervals in the presence of TMRE. The arrows indicate mitochondria that showed flickering. Three frames from the time-lapse analysis are shown (please also see Movies EV1–EV4). Scale bar, 10 μ m.
- C–E The percentage of cells that showed flickering in 30 min. Values are average \pm SD ($n = 3$ experiments). In each experiment, 25–89 cells were analyzed.
- F Drp1-KO MEFs were treated with DMSO or 10 nM antimycin A or 10 ng/ml oligomycin or 10 μ M FCCP for 1 h. The mitochondrial membrane potential was analyzed using MitoLite NIR and flow cytometry.
- G Drp1-KO MEFs expressing L2-HA (induced for 16 h) were treated with 10 nM antimycin A along with 10 μ M FCCP. Western blotting was performed using the indicated antibodies. The asterisk indicates non-specific bands of anti-Oma1 antibodies.
- H Quantification of band intensity. Values are average \pm SD ($n = 3$).
- I Western blotting of Drp1-KO MEFs with or without 10 ng/ml oligomycin treatment. The asterisk indicates non-specific bands of anti-Oma1 antibodies.
- J Quantification of band intensity. Values are average \pm SD ($n = 3$).
- K WT MEFs carrying Su9-GFP were treated with DMSO or 10 ng/ml oligomycin for 1 h and viewed by laser scanning confocal microscopy for 30 min with 10-s intervals in the presence of TMRE. The arrows indicate mitochondria that showed flickering. Three frames from the time-lapse analysis are shown (please also see Movies EV1 and EV5). Scale bar, 10 μ m.
- L WT MEFs expressing L2-HA (induced for 16 h) were treated with 10 ng/ml oligomycin. Western blotting was performed using the indicated antibodies. The asterisk indicates non-specific bands of anti-Oma1 antibodies.
- M Quantification of band intensity. Values are average \pm SD ($n = 3$).

Data information: Significance was calculated using ANOVA with *post hoc* Tukey in (C and H) and Student's *t*-test in (D, E, J and M): * $P < 0.05$, ** $P < 0.01$, *** $P < 0.001$.

the membrane potential after FCCP addition and immediately bring it back to the normal level after washout. We also set the interval of FCCP addition similar to that of flickering in Drp1-KO MEFs. Specifically, we added FCCP (final 10 μ M) to the culture medium for 1 min and washed it out for 4 min (Fig 5A). We repeated this addition-removal cycle 15 times. This treatment led to repeated, transient loss of the membrane potential in WT MEFs, similar to flickering observed in Drp1-KO MEFs (Fig 5B and C).

Western blotting showed that the artificial flickering increases the conversion of L2-HA to S5-HA (Fig 5D and E, 1 min \times 15) in WT MEFs, similar to what was observed in Drp1-KO MEFs. Consistent with these results, artificial flickering decreased the levels of Oma1 as a readout of Oma1 activation (Fig 5D and E, 1 min \times 15). In contrast, a single FCCP treatment did not induce Opa1 cleavage or Oma1 activation (Fig 5D and E, 1 min). When WT MEFs were continuously incubated with FCCP for 15 min, most L2-HA was processed to S5-HA (Fig 5D and E, 15 min). These data suggest that flickering is sufficient to induce Opa1 processing through limited Oma1 activation.

Restoring Opa1 and Mfn1 in Drp1-KO MEFs induces extreme fusion of mitochondria

In addition to Opa1 cleavage, mitochondrial outer membrane proteins that mediate fusion, Mfn1 and Mfn2, underwent enhanced degradation in Drp1-KO MEFs (Figs 1B and C, and 6A and B). Since mitochondrial fusion mediated by Mfn1, but not Mfn2, requires Opa1 (Cipolat *et al*, 2004), we reasoned that decreased levels of Opa1 and Mfn1 might decrease mitochondrial fusion in Drp1-KO MEFs. This model predicts that restoring Opa1 and Mfn1 levels increases mitochondrial fusion in Drp1-KO MEFs. To test this prediction, we measured the connectivity of mitochondria as a readout for the fusion status of mitochondria using matrix-targeted Su9-photoconvertible monomeric Eos (Su9-Eos) (Zhang *et al*, 2012), as we have performed using Su9-photoactivatable GFP (Roy *et al*, 2016). WT and Drp1-KO MEFs were transduced with Su9-Eos along with Oma1 shRNAs and ectopic Mfn1. shRNA-mediated Oma1 knockdown increased levels of unprocessed Opa1 in Drp1-KO

MEFs while ectopic expression of Mfn1 restored its normal level (Fig 6A and B).

We then illuminated single mitochondrion with a short pulse of laser to photoconvert Su9-Eos on the scanning laser confocal microscope (Fig 6C and D). Photoconverted red fluorescence of Su9-Eos was diffused into the connected matrix space, labeling a single mitochondrion. Within one second after illumination, we took images for unconverted green and photoconverted red Su9-Eos signals (Fig 5C and D). By dividing the area of photoconverted Su9-Eos signals by that of both photoconverted and unconverted Su9-Eos signals, we calculated the relative area of a single mitochondrion containing converted Su9-Eos (Fig 6E and F). The relative area was used to calculate the number of mitochondria in each cell (Fig 6G). We estimated that WT and Drp1-KO MEFs contain about 250 and 25 mitochondria on average, respectively (Fig 6G). The number of mitochondria in WT MEFs was not affected by Oma1 shRNAs. Ectopic expression of Mfn1 increased its levels by fivefold (Fig 6A and B) and decreased the number of mitochondria to approximately 150 (Fig 6G and H). Additional Oma1 shRNAs further lowered the number of mitochondria to roughly 100 (which was still higher than that of mitochondria in Drp1-KO MEFs) (Fig 6G and H). In contrast, in Drp1-KO MEFs, the number of mitochondria was decreased to about 10 only when both Oma1 shRNAs and ectopic Mfn1 are introduced (Fig 6G and H). Ectopic expression of Mfn1 restored its normal level without overexpression (Fig 6A and B). These data suggest that a combination of Opa1 cleavage and Mfn1 degradation decreases mitochondrial fusion in Drp1-KO MEFs and that both proteolytic mechanisms need to be lifted in order to restore mitochondrial fusion. To distinguish from hyperfusion, the further increased connectivity of mitochondria induced by restoring Opa1 long forms and Mfn1 in the absence of division was termed extreme fusion of mitochondria (Fig 6H).

Extreme fusion of mitochondria results in bioenergetic deficits

To test the impact of extreme fusion on mitochondrial function, we analyzed the mitochondrial membrane potential using TMRE staining in WT and Drp1-KO MEFs, in which Oma1 shRNAs and ectopic

Mfn1 are expressed. In WT MEFs, Oma1 knockdown and ectopic Mfn1 expression, whether individually or in combination, did not affect TMRE staining (Fig 7A and B). In contrast, in Drp1-KO MEFs, simultaneous expression of Oma1 shRNA and ectopic Mfn1 resulted in the loss of the membrane potential in approximately 50% of cells (Fig 7C and D)—interestingly, when we examined the MEFs that maintained the membrane potential, they showed flickering, similar to Drp1-KO MEFs (Appendix Fig S7). Single Oma1 knockdown or

Mfn1 expression did not decrease the membrane potential or flickering in Drp1-KO MEFs (Fig 7C and D, and Appendix Fig S7). In contrast to Mfn1, ectopic expression of Mfn2, in combination with Oma1 knockdown, did not lead to the loss of the membrane potential (Appendix Fig S8). These data suggest that, although Mfn1 and Mfn2 are homologous proteins, Mfn1 specifically mediates extreme fusion together with Opa1, consistent with previous studies (Cipolat et al, 2004).

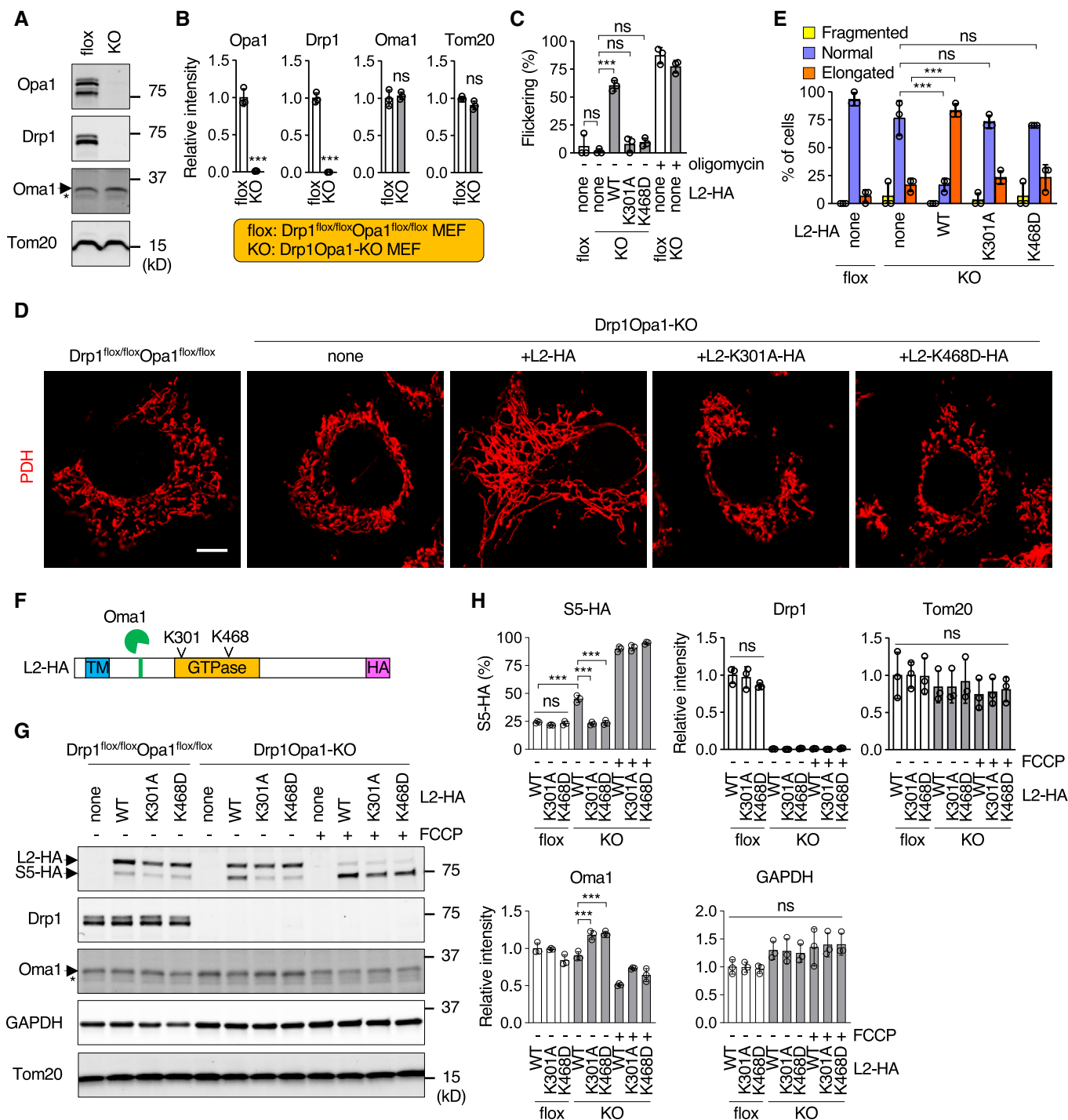
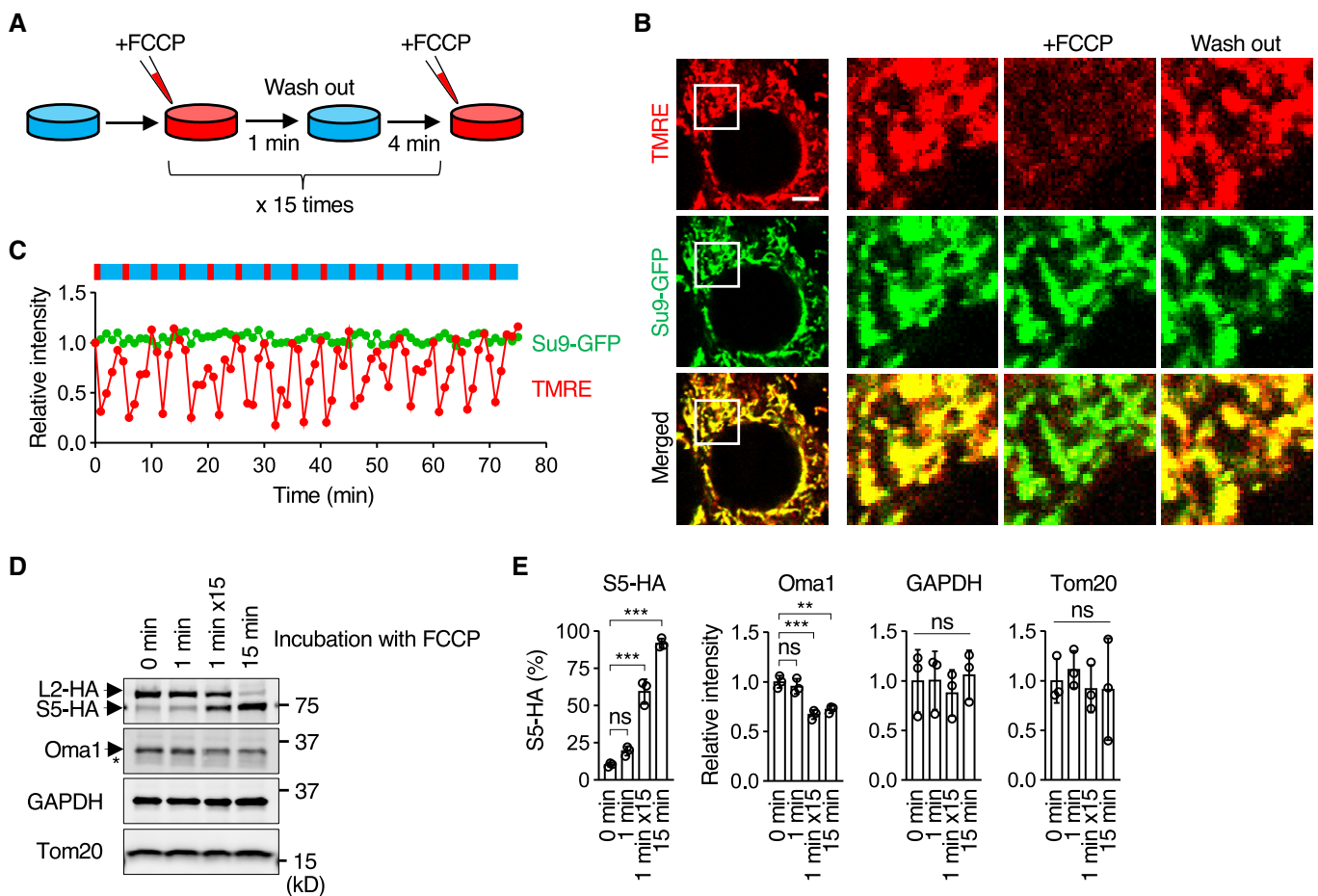


Figure 4.

Figure 4. The loss of Opa1 function decreases flickering and Opa1 cleavage in the absence of Drp1.

- A Western blotting of Drp1^{flox/flox}Opa1^{flox/flox} and Drp1Opa1-KO MEFs. The asterisk indicates non-specific bands of anti-Oma1 antibodies.
- B Quantification of band intensity. Values are average \pm SD ($n = 3$).
- C Drp1^{flox/flox}Opa1^{flox/flox} MEFs and Drp1Opa1-KO MEFs were transduced with the indicated Opa1 constructs. The cells were observed using laser scanning confocal microscopy for 30 min with 10-s intervals in the presence of TMRE. The percentage of cells that exhibited flickering is shown. Values are average \pm SD ($n = 3$ experiments). In each experiment, 48–62 cells were analyzed.
- D Drp1^{flox/flox}Opa1^{flox/flox} MEFs and Drp1Opa1-KO MEFs carrying the indicated Opa1 constructs were subjected to confocal immunofluorescence microscopy using anti-PDH antibodies. Scale bar, 10 μ m.
- E Quantification of mitochondrial morphology is shown ($n = 3$ experiments). In each experiment, 30 cells were analyzed.
- F L2-HA constructs carrying a mutation (K301A or K468D) in the GTPase domain.
- G Western blotting of Drp1^{flox/flox}Opa1^{flox/flox} MEFs and Drp1Opa1-KO MEFs, both of which carry the indicated Opa1 constructs. The asterisk indicates non-specific bands of anti-Oma1 antibodies.
- H Quantification of band intensity. Values are average \pm SD ($n = 3$).

Data information: Significance was calculated using Student's *t*-test in (B) and ANOVA with *post hoc* Tukey in (C, E, and H); *** $P < 0.001$.

**Figure 5. Artificial flickering induces Opa1 cleavage.**

- A Experimental design for artificial flickering. WT MEFs expressing Su9-GFP were subjected to repetitive FCCP treatments and observed using confocal microscopy in the presence of TMRE.
- B Three frames from the time-lapse analysis during artificial flickering are shown. The boxed regions are magnified. Scale bar, 5 μ m.
- C The fluorescence intensity of Su9-GFP and TMRE in mitochondria was quantified.
- D Western blotting of WT MEFs after the indicated FCCP treatments. The asterisk indicates non-specific bands of anti-Oma1 antibodies.
- E Quantification of band intensity. Values are average \pm SD ($n = 3$). Significance was calculated using ANOVA with *post hoc* Tukey. ** $P < 0.01$, *** $P < 0.001$.

Consistent with these data, a combination of Oma1 knockdown and Mfn1 expression strongly decreased both basal OCRs and respiratory capacity in Drp1-KO MEFs (Fig 7G and H). Again,

single Oma1 knockdown or Mfn1 expression did not decrease OCRs (Fig 7G and H). In WT MEFs, basal OCRs were only modestly decreased by Oma1 knockdown and Mfn1 expression

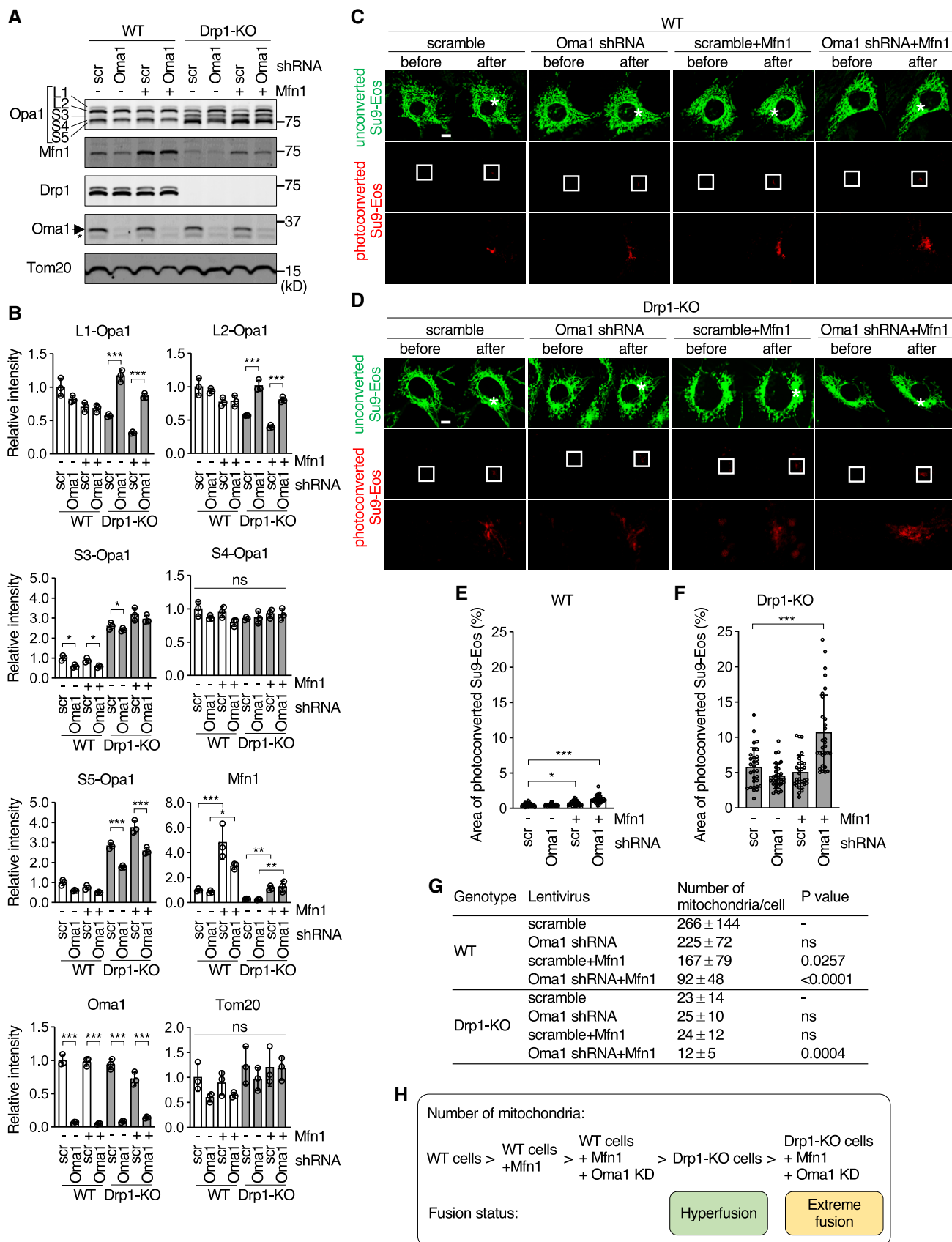


Figure 6.

Figure 6. Restoring Opa1 long forms and Mfn1 induces extreme fusion of mitochondria in Drp1-KO MEFs.

- A Western blotting of WT MEFs and Drp1-KO MEFs, both of which carry shRNAs (Oma1 or scramble) and/or ectopic Mfn1. The asterisk indicates non-specific bands of anti-Oma1 antibodies.
- B Quantification of band intensity is shown. Values are average \pm SD ($n = 3$).
- C–F WT MEFs (C and E) and Drp1-KO MEFs (D and F) were transduced with Su9-Eos, along with Oma1 shRNAs and ectopic Mfn1. Su9-Eos in the small region of mitochondria (indicated by the asterisks) was photoconverted using a 405-nm laser on confocal microscope. Within 1 s after photoconversion, images were obtained for both photoconverted and unconverted Su9-Eos signals. Images before the photoconversion were also taken to detect background signals. Scale bar, 10 μ m. (E and F) To determine the connectivity of mitochondria, the area containing photoconverted Su9-Eos signals was divided by the area containing the photoconverted and unconverted Su9-Eos signals (total mitochondria). Values are average \pm SD ($n = 30$ cells).
- G The number of mitochondria was estimated by reversing the connectivity.
- H Summary of the data.

Data information: Significance was calculated using ANOVA with *post hoc* Tukey in (B) and the Kruskal–Wallis test with *post hoc* Dunn in (E–G): * $P < 0.05$, ** $P < 0.01$, *** $P < 0.001$.

(Fig 7E and F). However, apoptosis was not increased by extreme fusion of mitochondria (Appendix Fig S9). These data suggest that extreme fusion decreases the respiratory function of mitochondria. It appears that proteolytic inhibition of Opa1 and Mfn1 prevents the harmful transition of mitochondrial connectivity from hyperfusion to extreme fusion to maintain mitochondrial bioenergetics (Fig 7I).

Knockout of Oma1 blocks increased Opa1 processing in Drp1-KO livers in mice

To test the physiological relevance of our findings, we tested whether Oma1 is required for increased processing of Opa1 in mice (Fig 8A and B). Since we have previously found that the loss of Drp1 increases Opa1 processing in the liver of liver-specific Drp1-KO mice (*Alb-Cre::Drp1^{fllox/fllox}* mice) (Yamada et al, 2018), we created *Oma1^{-/-}::Alb-Cre::Drp1^{fllox/fllox}* mice by breeding liver-specific Drp1-KO mice and Oma1-KO mice (*Oma1^{-/-}*) (Quiros et al, 2012; Yamada et al, 2018) and analyzed Opa1 processing in the liver from control (*Drp1^{fllox/fllox}*), Drp1-KO, Oma1-KO, and Drp1Oma1-KO mice. We found that the production of both S3 and S5 was increased in Drp1-KO livers in an Oma1-dependent manner (Fig 8A and B). These data suggest that the conversion of Opa1 long forms in the absence of Drp1 requires Oma1 *in vivo*.

Discussion

Flickering—repeated, transient decreases of the membrane potential—has been observed in multiple cell types, including smooth muscle cells (Chalmers et al, 2015), cardiomyocytes (Duchen et al, 1998), and a neuroblastoma cell line (Loew et al, 1993). In this study, we show that flickering induces Oma1-mediated Opa1 cleavage when mitochondrial division is decreased. Our data suggest that this Opa1 cleavage, along with the degradation of Mfn1, protects mitochondria from deleterious extreme fusion that leads to decreases in mitochondrial respiratory function (Fig 7I). The activation of Oma1 is regulated by flickering in the absence of mitochondrial division. Flickering enables the limited activation of Oma1 without losing the overall membrane potential and thereby allows the maintenance of the bioenergetic competence of mitochondria when the balance is shifted to excess connectivity. Decreased mitochondrial division is associated with many human

diseases affecting neurons and hepatocytes (Roy et al, 2015; Kameoka et al, 2018). We predict that the safeguard mechanisms against excess fusion are activated under these pathological conditions to prevent extreme fusion. If these protections are compromised, the disease phenotypes might become more severe. The strength of the protections might vary among cell types, and such differences likely contribute to cell-type specificity to diseases that affect mitochondrial division.

Multiple lines of experiments support the role of flickering for the Opa1 cleavage. First, by using the two drugs which inhibit or activate flickering, we show that the inhibition of flickering decreases Opa1 processing while its activation enhances it. Specifically, the Complex III inhibitor, antimycin A, inhibits flickering and Opa1 cleavage. On the other hand, when we stimulated flickering using the Complex V inhibitor, oligomycin, Opa1 cleavage was accelerated. Changes in Opa1 processing are not a consequence of global changes in the membrane potential or mitochondrial respiration. Although these two inhibitors can affect electron transport activities, neither antimycin A nor oligomycin decreased the overall membrane potential at the concentrations and timescales used in our experiments. Also, while antimycin A and oligomycin elicited the opposite effects on flickering and Opa1 cleavage, both inhibitors decreased OCRs. Therefore, decreased OCRs do not lead to Opa1 cleavage. Second, we suppressed flickering by deleting Opa1 in Drp1-KO cells. This inhibition of flickering decreased Oma1 activation and Opa1 processing in Drp1Opa1-KO MEFs. Third, the artificial flickering in WT MEFs by repeated cycles of addition and removal of FCCP-induced Oma1 activation and Opa1 processing. These data suggest that flickering controls Oma1-mediated Opa1 cleavage in the absence of mitochondrial division.

We have previously shown that flickering occurs in matrix-connected mitochondria in Drp1-KO MEFs by concomitantly visualizing the membrane potential using TMRE and the matrix connectivity using photoactivatable Su9-GFP (Roy et al, 2016). When mitochondrial division is blocked, this depolarization spreads through the connected mitochondria, but does not propagate to neighboring mitochondria, in Drp1-KO MEFs. Therefore, each flickering event is constrained in individual mitochondria (Roy et al, 2016). Interestingly, a recent study has shown that, even within a single mitochondrion, the membrane potential is individually maintained in each cristae structure, separately from neighboring cristae (Wolf et al, 2019). This individual electrical integrity of cristae requires Opa1 (Wolf et al, 2019). Therefore, Opa1 cleavage

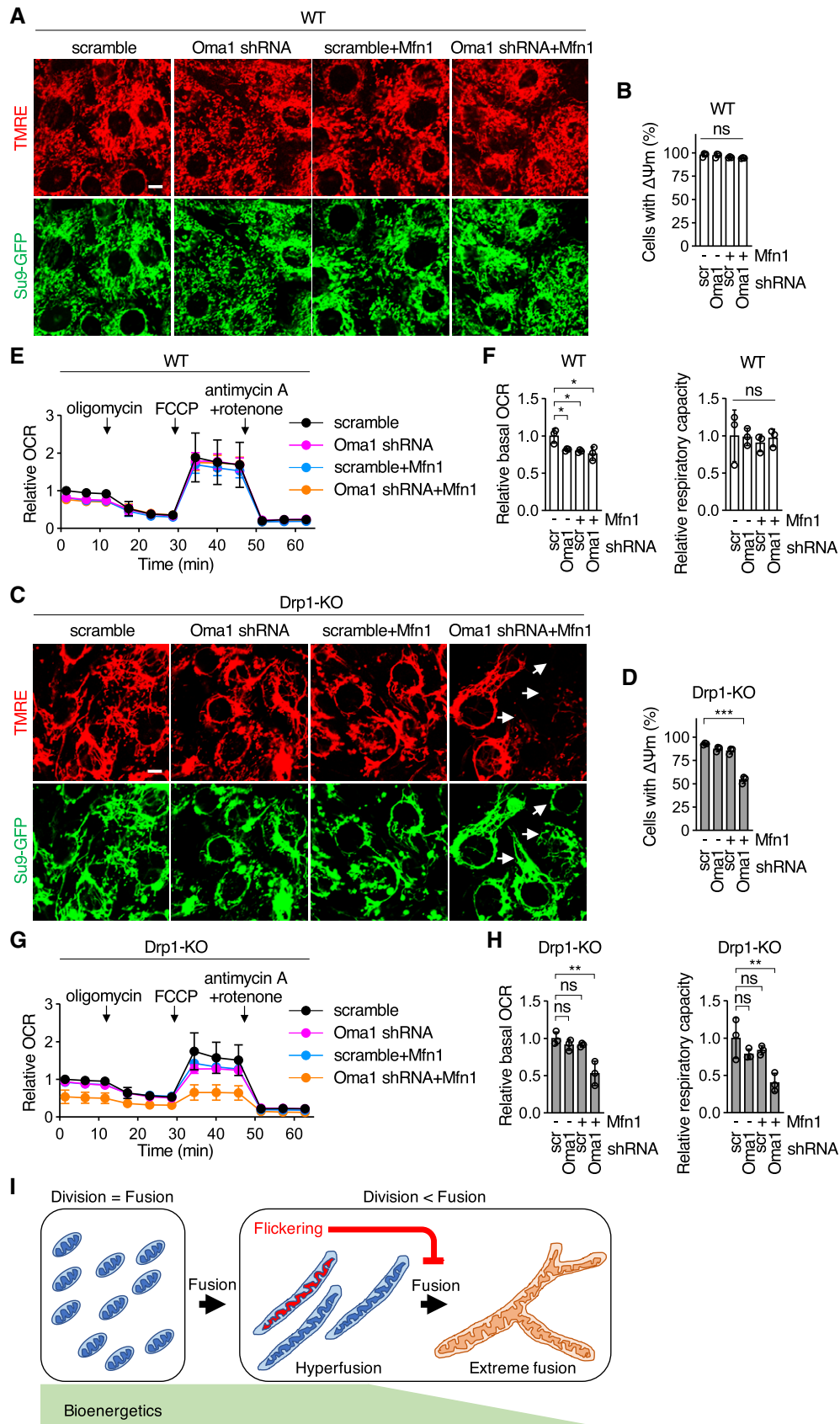


Figure 7.

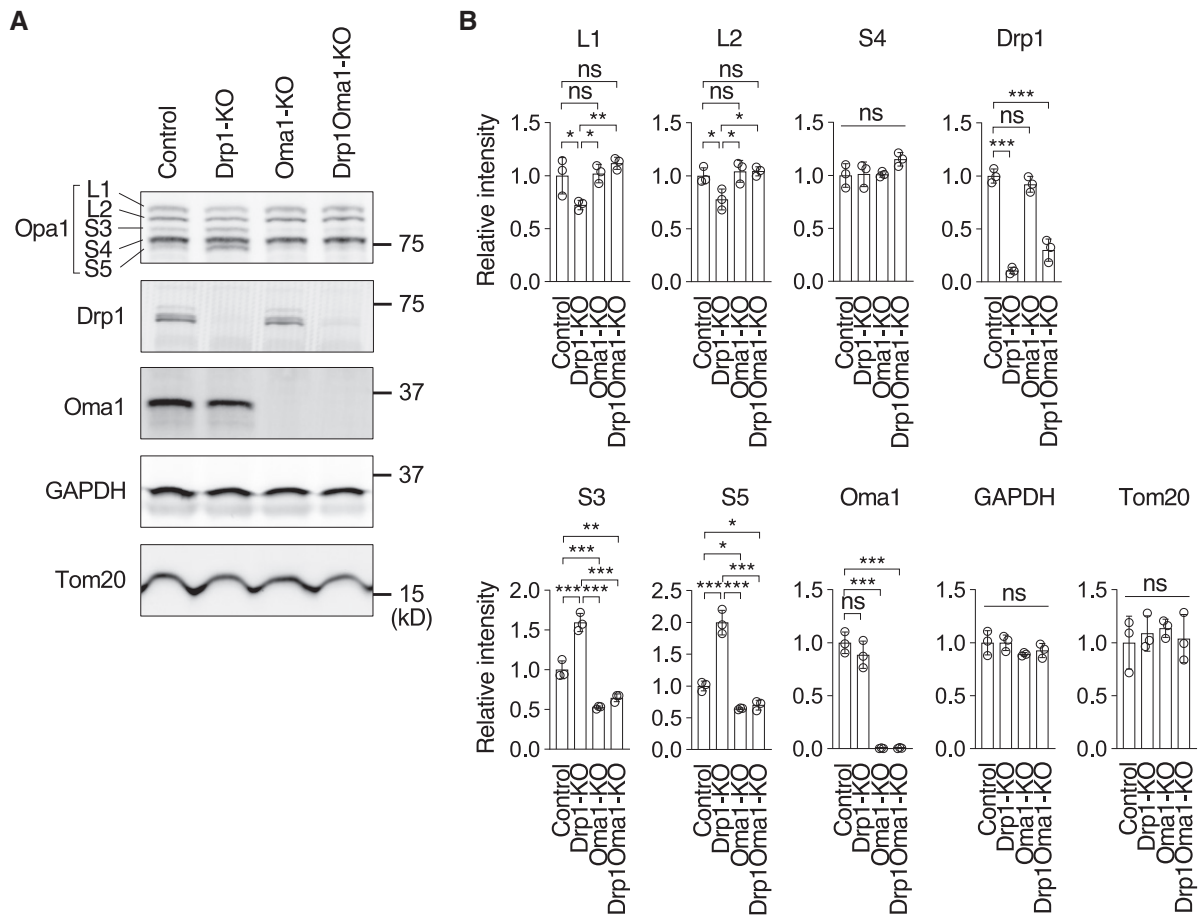
Figure 7. Extreme mitochondrial fusion decreases the membrane potential and respiration.

A–D WT (A and B) and Drp1-KO MEFs (C and D), both of which carry shRNAs (Oma1 or scramble) and ectopic Mfn1, were stained with TMRE. The arrows indicate cells that lost the mitochondrial membrane potential in (C). Scale bar, 10 μ m. (B and D) The percentage of cells that maintained the membrane potential is shown. Values are average \pm SD ($n = 3$). 100–150 cells were analyzed in each experiment.

E–H OCRs were analyzed in the same set of MEFs. (F and H) Quantification of the basal OCRs and respiratory capacity is shown. Values are average \pm SD ($n = 3$).

I Summary of the data.

Data information: Significance was calculated using ANOVA with *post hoc* Tukey in (B, D, F, and H): * $P < 0.05$, ** $P < 0.01$, *** $P < 0.001$.

**Figure 8. Knockout of Oma1 blocks increases in Opa1 processing in Drp1-KO livers in mice.**

A Western blotting of livers isolated from the indicated mice at 3 months of age using the indicated antibodies.

B Quantification of band intensity. Values are average \pm SD ($n = 3$ mice for each genotype). Significance was calculated using ANOVA with *post hoc* Tukey: * $P < 0.05$, ** $P < 0.01$, *** $P < 0.001$.

in Drp1-KO MEFs may facilitate synchronized, transient loss of the membrane potential in multiple cristae by losing their electrical individuality.

It has been suggested that proton leak through unidentified pores in the inner membrane depolarizes the membrane and causes flickering (Galloway *et al*, 2012; Lee & Yoon, 2014). For example, the mitochondrial permeability transition pore could be a candidate molecule that mediates flickering; however, its inhibitor, cyclosporin A, did not block flickering (Lee & Yoon, 2014). In our previous study, we have shown that drugs that change calcium signaling do not affect flickering in Drp1-KO MEFs,

including thapsigargin (an inhibitor of endoplasmic reticulum Ca^{2+} ATPase), BAPTA-AM (a calcium chelator), and Ru360 (mitochondrial calcium uniporter) (Roy *et al*, 2016). Also, we have shown that genipin (inhibitor of uncoupling protein 2) does not change flickering in Drp1-KO MEFs. These data suggest that calcium signaling and uncoupling protein are not involved in flickering in Drp1-KO MEFs. It would be of great interest to decipher the identity of the missing transporter in order to better understand how mitochondrial division controls flickering and how antimycin A and oligomycin modulate the activity of such transporters in future studies.

Materials and Methods

Animals

All animal work was performed according to the guideline established by the Johns Hopkins University Committee on Animal Care. Control (*Drp1^{flox/flox}*), liver-specific *Drp1*-KO (*Alb-Cre::Drp1^{flox/flox}*), *Oma1*-KO (*Oma1^{-/-}*), and *Drp1**Oma1*-KO (*Alb-Cre::Drp1^{flox/flox}::Oma1^{-/-}*) mice were generated by breeding (Quiros *et al*, 2012; Yamada *et al*, 2018).

Cells

HEK293T cells were cultured in Dulbecco's Modified Eagle Medium containing 10% fetal bovine serum. MEFs were cultured in Iscove's modified Dulbecco's medium containing 10% fetal bovine serum (Wakabayashi *et al*, 2009). Stable cell lines expressing *Opa1*-HA were selected with 400 µg/ml G418 sulfate. To generate *Drp1**Opa1*-KO MEFs, *Drp1^{flox/flox}Opa1^{flox/flox}* MEFs were isolated from *Drp1^{flox/flox}Opa1^{flox/flox}* embryos as described previously (Yamada *et al*, 2018) and transduced with lentiviruses carrying both Cre and GFP. Transduced cells were collected by fluorescence-activated cell sorting based on GFP expression. *Mff*-KO MEFs were generated using a GeneArt CRISPR Nuclease (OFP Reporter) Vector Kit (A21174; Thermo Fisher Scientific) in accordance with manufacturer's instructions. The target gRNA sequence was 5'-TGGGACTTGCAT TATCACAC-3'.

Plasmids

To generate tetracycline-inducible lentiviral vectors carrying *Opa1*-HA, human *Opa1* isoform1 (www.uniprot.org) was cloned into the pENTR/D-TOPO plasmid using pENTR Directional TOPO Cloning Kits (Thermo Fisher Scientific). The mutant *Opa1*(K301A and K468D) plasmids were generated by replacing the nucleotides (901A>G and 902A>C for K301A and 1402A>G and 1404A>C for K468D) in the WT *Opa1* plasmid. First, two partial fragments of *Opa1* were PCR-amplified from the *Opa1*(WT) plasmid using the following primers. K301A: 5'-CACCGCCACCATGTGGCGACTACGTC GGG-3' and 5'-AATCATTTCCAACACACTAGTCGCTCCAG-3', and 5'-CTAGTGTGTTGGAAATGATTGCCAAG-3' and 5'-TTAAGCGTAAT CTGGAACATCGTATGGGTAACCTCCTCCTCCTTTCTCCTGATG AAGAGCTCAATGAAAG-3'. K468D: 5'-CACCGCCACCATGTGGCG ACTACGTCGGG-3' and 5'-ATTTTTCTCTGCCAGGTCTACGTCGGTC-3', and 5'-TAGACCTGGCAGAGAAAATGTAGCC-3' and 5'-TTAAG CGTAATCTGGAACATCGTATGGGTAACCTCCTCCTCCTTTCTC CTGATGAAGAGCTTCAATGAAAG-3'. Underlined cases indicate the introduced mutations. Second, the full length of the mutant *Opa1* was PCR-amplified from the two products of the first PCR using the following primers: 5'-CACCGCCACCATGTGGCGACTACGTCGGG-3' and 5'-TTAAGCGTAATCTGGAACATCGTATGGGTAACCTCCTCCTCCTCCTttctctgatgaagagcttcaatgaaag-3'.

The *Opa1*-HA was then moved into the pInducer20 plasmid using the Gateway LR Clonase II Enzyme Mix (Thermo Fisher Scientific). To induce the expression of *Opa1*-HA, MEFs were incubated with 0.1 µg/ml doxycycline for 16 h. To generate shRNA plasmids, the following target sequences were cloned into pLKO.1. Scramble: CCTAAGGTTAAGTCGCCCTCGctcgagCGAGGGCGACTTAACCTTAG

G, *Oma1*: GCTTGGTTCATTTACTGGATTctcgagAATCCAGTAAATG AACCAAGC, *Drp1*: GCTTCAGATCAGAGAACTTATctcgagATAAGTT CTCTGATCTGAAGC. *Mic60*: GCCTGTACCAATACTTCCTTTctcgagA AAGGAAGTATTGGTACAGGC.

Lentivirus

Lentiviruses were generated as described previously (Kageyama *et al*, 2014). HEK293T cells were seeded at 1.5×10^6 cells in a 10-cm dish and cultured for 24 h. To produce lentiviruses, 3 µg of the pHR-Sin plasmid carrying Su9-GFP or Su9-Eos 3.2, or the pInducer20 plasmid carrying *Opa1*-HA, or the FUW-GFP plasmid carrying Cre, or pLKO.1 carrying scramble, *Oma1*, *Drp1* or *Mic60* shRNAs was co-transfected into HEK293T cells along with 3 µg of pHR-CMV8.2ΔR for pHR-Sin and pLKO.1 (or pHR-CMV8.9ΔR for pInducer20 and FUW-GFP) and 0.3 µg of pCMV-VSVG by using Lipofectamine 2000 (Invitrogen). After 20–22 h, the culture medium was replaced with fresh medium. After an additional 24 h, the culture medium containing released viruses was collected. Lentiviruses carrying *Opa1*-HA or Cre were concentrated using Lenti-X Concentrator (Clontech). For lentiviral transduction, MEFs were seeded at 8×10^4 cells/well in a 6-well plate and cultured for 24 h. Cells were then incubated with lentivirus in IMDM containing 10% FBS and 8 µg/ml polybrene for 24 h.

Western blotting

Cells were harvested and lysed in RIPA buffer (9806S, Cell Signaling Technology) supplemented with cComplete, Mini, EDTA-free Protease Inhibitor Cocktail (11836170001, Roche) on ice. Mouse livers were harvested, flash-frozen in liquid nitrogen, and homogenized in the RIPA buffer on ice. The lysates were centrifuged at 16,000 g for 10 min at 4°C, and the supernatants were collected. Proteins were separated by SDS-PAGE and transferred onto Immobilon-FL Transfer Membrane (Millipore). The membranes were blocked in PBS-T (PBS containing 0.05% Tween 20) containing 3% BSA at room temperature for 1 h and then incubated with primary antibodies in PBS-T containing 3% BSA at 4°C overnight. The antibodies used were *Opa1* (1:1,000 dilution, 612607; BD Biosciences), *Drp1* (1:2,000 dilution, 611113; BD Biosciences), *GAPDH* (1:10,000 dilution, MA5-15738; Thermo Fisher Scientific), *Tom20* (1:2,000 dilution, sc-11415; Santa Cruz Biotechnology), *HA* (1:2,000 dilution, NB600-362; Novus Biologicals), *Oma1* (1:1,000 dilution, sc-515788; Santa Cruz Biotechnology), *mitofusin 1* (1:1,000 dilution, ab126575; Abcam), *mitofusin 2* (1:1,000 dilution, ab57602; Abcam), *Mff* (1:1,000 dilution, gifted from Dr. Alexander M. van der Blik, UCLA, USA), *Fis1* (1:2,000 dilution, 10956-1-AP; ProteinTech), *Mid49* (1:1,000 dilution, 16413-1-AP; ProteinTech), *Mid51* (1:1,000 dilution, 20164-1-AP; ProteinTech), *Mic60* (1:1,000 dilution, 10179-1-AP; ProteinTech), *PARP1* (1:1,000 dilution, 9542; Cell Signaling Technology), and *Caspase-3* (1:1,000 dilution, 9665; Cell Signaling Technology). The membranes were washed three times in PBS-T, followed by incubation with appropriate secondary antibodies at room temperature for 1 h. After washing the membranes three times in PBS-T, fluorescence signals were detected using a PharosFX Plus Molecular Imager (Bio-Rad).

Flickering assay

MEFs carrying Su9-GFP were seeded at 40,000 cells/well in 8-well chambered coverglasses and cultured for 24 h. Cells were treated with DMSO, 10 nM antimycin A or 10 ng/ml oligomycin at 37°C with 5% CO₂ for 1 h. Cells were then stained with 5 nM TMRE in phenol red-free IMDM containing 10% FBS at 37°C with 5% CO₂ for 15 min and were examined using a Zeiss LSM800 GaAsP confocal microscope with a 40× objective lens at 37°C with 5% CO₂. To minimize potential phototoxicity, images were obtained with 10-s intervals for 30 min at a single focal plane.

Measurements of the mitochondrial membrane potential

The mitochondrial membrane potential was measured using Cell Meter NIR Mitochondrial Membrane Potential Assay Kit (AAT Bioquest) in accordance with the manufacturer's instructions. Briefly, MEFs were suspended in 1 ml of IMDM containing 10% FBS and treated with DMSO, 10 μM FCCP, 10 nM antimycin A, or 10 ng/ml oligomycin at 37°C with 5% CO₂ for 30 min. Cells were then incubated with MitoLite NIR at 37°C and 5% CO₂ for 30 min. Cells were resuspended in 1 ml of the supplied assay buffer and then filtered through a 70 μm cell strainer (22363548, Fisher Scientific). The fluorescence intensity was measured by using a FACSCalibur (BD Biosciences).

Mitochondrial respiration

Mitochondrial OCRs were measured by using an XF96 Extracellular Flux Analyzer (Seahorse Bioscience) (Kageyama *et al*, 2014). Cells were seeded at 5,000 cells/well in an XF 96-well culture microplate and cultured for 24 h. Cells were washed twice in XF base medium supplemented with 25 mM glucose, 4 mM L-glutamine, and 1 mM sodium pyruvate. The culture medium was replaced with the XF base medium containing DMSO, 10 nM antimycin A, or 10 ng/ml oligomycin, and then cells were incubated at 37°C in a CO₂-free incubator for 1 h. OCR measurement was performed according to the manufacturer's instructions. Baseline OCR was recorded three times, and then, 1.6 μg/ml oligomycin, 1 μM FCCP, and 0.5 μM rotenone/antimycin A were sequentially injected into each well. OCRs were normalized relative to the amount of protein in each well.

The activity of electron transport chain complexes

Crude mitochondrial fractions were isolated from WT and Drp1 KO MEFs. MEFs at 90% confluence in two 10-cm dishes were suspended in 800 μl of homogenization buffer [10 mM HEPES-KOH, pH 7.4, containing 220 mM mannitol, 70 mM sucrose and cOmplete, EDTA-free Protease Inhibitor Cocktail (Roche)]. Cells were homogenized on ice with ten strokes using a 27-gauge needle attached to a plastic syringe. The homogenate was centrifuged at 200 g for 5 min at 4°C to remove cell debris and nuclei. The supernatant was centrifuged at 4,000 g for 5 min at 4°C to pellet the mitochondria-enriched fraction. The activities of Complexes III and V in the mitochondria-enriched fraction was measured using the MitoCheck Complex II/III Activity Assay Kit and MitoCheck Complex V Activity Assay Kit (Cayman Chemical), respectively, in accordance with manufacturer's instructions.

Immunofluorescence microscopy

MEFs were fixed in pre-warmed (37°C) PBS containing 4% paraformaldehyde for 20 min, washed three times in PBS, permeabilized with PBS containing 0.1% Triton X-100 for 8 min, washed again three times in PBS, and blocked in PBS containing 0.5% BSA at room temperature for 30 min (Adachi *et al*, 2016). Cells were then incubated with anti-PDH antibody (1:400 in PBS containing 0.5% BSA, ab110333, Abcam) and anti-Tom20 antibody (1:300 in PBS containing 0.5% BSA, sc-11415; Santa Cruz Biotechnology) at 4°C overnight. Cells were washed three times in PBS and incubated with Alexa 488-conjugated anti-mouse IgG (1:400 in PBS, A21202, Thermo Fisher Scientific) and Alexa 568-conjugated anti-rabbit IgG (1:400 in PBS, A10042, Thermo Fisher Scientific) at room temperature for 1 h. Cells were washed again, three times in PBS. The samples were observed using an LSM800 GaAsP laser scanning confocal microscope (Kageyama *et al*, 2014; Yamada *et al*, 2016). For composite images of mitochondria, 10 images at 0.3 μm intervals were acquired using a 63× objective lens and were compiled by average intensity projection and 3D viewer in Fiji software.

Photoconversion of Su9-Eos

MEFs carrying Su9-Eos were seeded at 10,000 cells/well in an 8-well chambered coverglasses and cultured for 24 h. Su9-Eos in 0.287 μm² of mitochondria was photoconverted for 6 s using a 405 nm laser on LSM800 GaAsP laser scanning confocal microscope. Images were obtained for both unconverted and photoconverted Su9-Eos signals before and after photoconversion using a 63× objective lens at a single focal plane. Images before the photoconversion were taken to detect background signals. Image analysis was performed using Fiji software. To determine the connectivity of mitochondria, the area containing photoconverted Su9-Eos signals was divided by the area containing the photoconverted and unconverted Su9-Eos signals (total mitochondria).

Chemical induction of apoptosis

Cells were seeded at 1.5×10^5 cells/well in 6-well plates and cultured for 24 h. Cells were then treated with 1 μM staurosporine or 50 μM etoposide for 6 or 22 h, respectively. Cells were harvested and lysed for Western blotting analysis.

Data availability

All data needed to evaluate the conclusions in the paper are present in the paper and/or the Expanded View files.

Expanded View for this article is available online.

Acknowledgements

We thank past and present members of the Iijima and Sesaki laboratories for helpful discussions and technical assistance. We are also grateful to Dr. Rong Li for providing the monomeric Eos plasmid. This work was supported by NIH grants to MI (GM131768) and HS (GM123266 and GM130695) and grants to HS from Diana Helis Henry Medical Research

Foundation and Adrienne Helis Malvin Medical Research Foundation and Robert J. Kleberg, Jr. and Helen C. Kleberg Foundation.

Author contributions

Project conception and study design: DM, MI, HS; Experiments and data analysis: DM, TY, TT, KA; Critical materials: PMQ, CL-O; Manuscript writing: DM, MI, HS.

Conflict of interest

The authors declare that they have no conflict of interest.

References

- Acin-Perez R, Lechuga-Vieco AV, Del Mar MM, Nieto-Arellano R, Torroja C, Sanchez-Cabo F, Jimenez C, Gonzalez-Guerra A, Carrascoso I, Beninca C et al (2018) Ablation of the stress protease OMA1 protects against heart failure in mice. *Sci Transl Med* 10: eaan4935
- Adachi Y, Itoh K, Yamada T, Cerveny KL, Suzuki TL, Macdonald P, Frohman MA, Ramachandran R, Iijima M, Sesaki H (2016) Coincident phosphatidic acid interaction restrains Drp1 in mitochondrial division. *Mol Cell* 63: 1034–1043
- Anand R, Wai T, Baker MJ, Kladt N, Schauss AC, Rugarli E, Langer T (2014) The i-AAA protease YME1L and OMA1 cleave OPA1 to balance mitochondrial fusion and fission. *J Cell Biol* 204: 919–929
- Baker MJ, Lampe PA, Stojanovski D, Korwitz A, Anand R, Tatsuta T, Langer T (2014) Stress-induced OMA1 activation and autocatalytic turnover regulate OPA1-dependent mitochondrial dynamics. *EMBO J* 33: 578–593
- Chalmers S, Saunter CD, Girkin JM, McCarron JG (2015) Flicker-assisted localization microscopy reveals altered mitochondrial architecture in hypertension. *Sci Rep* 5: 16875
- Cipolat S, Martins de Brito O, Dal Zilio B, Scorrano L (2004) OPA1 requires mitofusin 1 to promote mitochondrial fusion. *Proc Natl Acad Sci USA* 101: 15927–15932
- Dadgar S, Hagens O, Dadgar SR, Haghighi EN, Schimpf S, Wissinger B, Garshasbi M (2006) Structural model of the OPA1 GTPase domain may explain the molecular consequences of a novel mutation in a family with autosomal dominant optic atrophy. *Exp Eye Res* 83: 702–706
- Divakaruni SS, Van Dyke AM, Chandra R, LeGates TA, Contreras M, Dharmasri PA, Higgs HN, Lobo MK, Thompson SM, Blanpied TA (2018) Long-term potentiation requires a rapid burst of dendritic mitochondrial fission during induction. *Neuron* 100: 860–875.e7
- Duchen MR, Leysens A, Crompton M (1998) Transient mitochondrial depolarizations reflect focal sarcoplasmic reticular calcium release in single rat cardiomyocytes. *J Cell Biol* 142: 975–988
- Ehse S, Raschke I, Mancuso G, Bernacchia A, Geimer S, Tondera D, Martinou JC, Westermann B, Rugarli E, Langer T (2009) Regulation of OPA1 processing and mitochondrial fusion by m-AAA protease isoenzymes and OMA1. *J Cell Biol* 187: 1023–1036
- Friedman JR, Nunnari J (2014) Mitochondrial form and function. *Nature* 505: 335–343
- Galloway CA, Lee H, Nejjar S, Jhun BS, Yu T, Hsu W, Yoon Y (2012) Transgenic control of mitochondrial fission induces mitochondrial uncoupling and relieves diabetic oxidative stress. *Diabetes* 61: 2093–2104
- Griparic L, van der Wel NN, Orozco IJ, Peters PJ, van der Bliek AM (2004) Loss of the intermembrane space protein Mgm1/OPA1 induces swelling and localized constrictions along the lengths of mitochondria. *J Biol Chem* 279: 18792–18798
- Head B, Griparic L, Amiri M, Gandre-Babbe S, van der Bliek AM (2009) Inducible proteolytic inactivation of OPA1 mediated by the OMA1 protease in mammalian cells. *J Cell Biol* 187: 959–966
- Ishihara N, Nomura M, Jofuku A, Kato H, Suzuki SO, Masuda K, Otera H, Nakanishi Y, Nonaka I, Goto Y et al (2009) Mitochondrial fission factor Drp1 is essential for embryonic development and synapse formation in mice. *Nat Cell Biol* 11: 958–966
- Itoh K, Nakamura K, Iijima M, Sesaki H (2013) Mitochondrial dynamics in neurodegeneration. *Trends Cell Biol* 23: 64–71
- Kageyama Y, Zhang Z, Roda R, Fukaya M, Wakabayashi J, Wakabayashi N, Kensler TW, Reddy PH, Iijima M, Sesaki H (2012) Mitochondrial division ensures the survival of postmitotic neurons by suppressing oxidative damage. *J Cell Biol* 197: 535–551
- Kageyama Y, Hoshijima M, Seo K, Bedja D, Sysa-Shah P, Andrabi SA, Chen W, Hoke A, Dawson VL, Dawson TM et al (2014) Parkin-independent mitophagy requires Drp1 and maintains the integrity of mammalian heart and brain. *EMBO J* 33: 2798–2813
- Kameoka S, Adachi Y, Okamoto K, Iijima M, Sesaki H (2018) Phosphatidic acid and cardiolipin coordinate mitochondrial dynamics. *Trends Cell Biol* 28: 67–76
- Kashatus DF (2018) The regulation of tumor cell physiology by mitochondrial dynamics. *Biochem Biophys Res Commun* 500: 9–16
- Kleiner DE, Makhlof HR (2016) Histology of nonalcoholic fatty liver disease and nonalcoholic steatohepatitis in adults and children. *Clin Liver Dis* 20: 293–312
- Kraus F, Ryan MT (2017) The constriction and scission machineries involved in mitochondrial fission. *J Cell Sci* 130: 2953–2960
- Lee H, Yoon Y (2014) Transient contraction of mitochondria induces depolarization through the inner membrane dynamin OPA1 protein. *J Biol Chem* 289: 11862–11872
- Li Z, Okamoto K, Hayashi Y, Sheng M (2004) The importance of dendritic mitochondria in the morphogenesis and plasticity of spines and synapses. *Cell* 119: 873–887
- Liesa M, Shirihai OS (2013) Mitochondrial dynamics in the regulation of nutrient utilization and energy expenditure. *Cell Metab* 17: 491–506
- Loew LM, Tuft RA, Carrington W, Fay FS (1993) Imaging in five dimensions: time-dependent membrane potentials in individual mitochondria. *Biophys J* 65: 2396–2407
- MacVicar T, Langer T (2016) OPA1 processing in cell death and disease – the long and short of it. *J Cell Sci* 129: 2297–2306
- McNiven MA, Cao H, Pitts KR, Yoon Y (2000) The dynamin family of mechanoenzymes: pinching in new places. *Trends Biochem Sci* 25: 115–120
- Mopert K, Hajek P, Frank S, Chen C, Kaufmann J, Santel A (2009) Loss of Drp1 function alters OPA1 processing and changes mitochondrial membrane organization. *Exp Cell Res* 315: 2165–2180
- Pernas L, Scorrano L (2016) Mito-morphosis: mitochondrial fusion, fission, and cristae remodeling as key mediators of cellular function. *Annu Rev Physiol* 78: 505–531
- Prudent J, McBride HM (2017) The mitochondria-endoplasmic reticulum contact sites: a signalling platform for cell death. *Curr Opin Cell Biol* 47: 52–63
- Quiros PM, Ramsay AJ, Sala D, Fernandez-Vizarra E, Rodriguez F, Peinado JR, Fernandez-Garcia MS, Vega JA, Enriquez JA, Zorzano A et al (2012) Loss of mitochondrial protease OMA1 alters processing of the GTPase OPA1 and causes obesity and defective thermogenesis in mice. *EMBO J* 31: 2117–2133

- Rainbolt TK, Lebeau J, Puchades C, Wiseman RL (2016) Reciprocal degradation of YME1L and OMA1 adapts mitochondrial proteolytic activity during stress. *Cell Rep* 14: 2041–2049
- Ramachandran R (2018) Mitochondrial dynamics: The dynamin superfamily and execution by collusion. *Semin Cell Dev Biol* 76: 201–212
- Roy M, Reddy PH, Iijima M, Sesaki H (2015) Mitochondrial division and fusion in metabolism. *Curr Opin Cell Biol* 33C: 111–118
- Roy M, Itoh K, Iijima M, Sesaki H (2016) Parkin suppresses Drp1-independent mitochondrial division. *Biochem Biophys Res Commun* 475: 283–288
- Saita S, Ishihara T, Maeda M, Iemura S, Natsume T, Mihara K, Ishihara N (2016) Distinct types of protease systems are involved in homeostasis regulation of mitochondrial morphology via balanced fusion and fission. *Genes Cells* 21: 408–424
- Serasinghe MN, Chipuk JE (2017) Mitochondrial fission in human diseases. *Handb Exp Pharmacol* 240: 159–188
- Sesaki H, Jensen RE (1999) Division versus fusion: Dnm1p and Fzo1p antagonistically regulate mitochondrial shape. *J Cell Biol* 147: 699–706
- Sesaki H, Jensen RE (2001) UGO1 encodes an outer membrane protein required for mitochondrial fusion. *J Cell Biol* 152: 1123–1134
- Sesaki H, Southard SM, Yaffe MP, Jensen RE (2003) Mgm1p, a dynamin-related GTPase, is essential for fusion of the mitochondrial outer membrane. *Mol Biol Cell* 14: 2342–2356
- Shields LY, Kim H, Zhu L, Haddad D, Berthet A, Pathak D, Lam M, Ponnusamy R, Diaz-Ramirez LG, Gill TM et al (2015) Dynamin-related protein 1 is required for normal mitochondrial bioenergetic and synaptic function in CA1 hippocampal neurons. *Cell Death Dis* 6: e1725
- Song Z, Chen H, Fiket M, Alexander C, Chan DC (2007) OPA1 processing controls mitochondrial fusion and is regulated by mRNA splicing, membrane potential, and Yme1L. *J Cell Biol* 178: 749–755
- Stephan T, Bruser C, Deckers M, Steyer AM, Balzarotti F, Barbot M, Behr TS, Heim G, Hubner W, Ilgen P et al (2020) MICOS assembly controls mitochondrial inner membrane remodeling and crista junction redistribution to mediate cristae formation. *EMBO J* 39: e104105
- Tamura Y, Itoh K, Sesaki H (2011) SnapShot: Mitochondrial dynamics. *Cell* 145: 1158
- Twig G, Elorza A, Molina AJ, Mohamed H, Wikstrom JD, Walzer G, Stiles L, Haigh SE, Katz S, Las G et al (2008) Fission and selective fusion govern mitochondrial segregation and elimination by autophagy. *EMBO J* 27: 433–446
- van der Blik AM, Shen Q, Kawajiri S (2013) Mechanisms of mitochondrial fission and fusion. *Cold Spring Harb Perspect Biol* 5: a011072
- Wakabayashi J, Zhang Z, Wakabayashi N, Tamura Y, Fukaya M, Kensler TW, Iijima M, Sesaki H (2009) The dynamin-related GTPase Drp1 is required for embryonic and brain development in mice. *J Cell Biol* 186: 805–816
- Widlansky ME, Hill RB (2018) Mitochondrial regulation of diabetic vascular disease: an emerging opportunity. *Transl Res* 202: 83–98
- Wolf DM, Segawa M, Kondadi AK, Anand R, Bailey ST, Reichert AS, van der Blik AM, Shackelford DB, Liesa M, Shirihai OS (2019) Individual cristae within the same mitochondrion display different membrane potentials and are functionally independent. *EMBO J* 38: e101056
- Yamada T, Adachi Y, Fukaya M, Iijima M, Sesaki H (2016) Dynamin-related protein 1 deficiency leads to receptor-interacting protein kinase 3-mediated necroptotic neurodegeneration. *Am J Pathol* 86: 2798–2802
- Yamada T, Murata D, Adachi Y, Itoh K, Kameoka S, Igarashi A, Kato T, Araki Y, Haganir RL, Dawson TM et al (2018) Mitochondrial stasis reveals p62-mediated ubiquitination in Parkin-independent mitophagy and mitigates nonalcoholic fatty liver disease. *Cell Metab* 28: 588–604
- Yamada T, Dawson TM, Yanagawa T, Iijima M, Sesaki H (2019) SQSTM1/p62 promotes mitochondrial ubiquitination independently of PINK1 and PRKN/parkin in mitophagy. *Autophagy* 15: 2012–2018
- Youle RJ, van der Blik AM (2012) Mitochondrial fission, fusion, and stress. *Science* 337: 1062–1065
- Zhang M, Chang H, Zhang Y, Yu J, Wu L, Ji W, Chen J, Liu B, Lu J, Liu Y et al (2012) Rational design of true monomeric and bright photoactivatable fluorescent proteins. *Nat Methods* 9: 727–729
- Zhang K, Li H, Song Z (2014) Membrane depolarization activates the mitochondrial protease OMA1 by stimulating self-cleavage. *EMBO Rep* 15: 576–585